New Journal of Physics
The open access journal for physics

Nonlinear emission characteristics of quantum dot–micropillar lasers in the presence of polarized optical feedback

C Hopfmann[1,3], F Albert[1], C Schneider[1], S Höfling[1], M Kamp[1], A Forchel[1], I Kanter[2] and S Reitzenstein[1,3,4]

[1] Technische Physik, Universität Würzburg and Wilhelm Conrad Röntgen Research Center for Complex Material Systems, Am Hubland, D-97074 Würzburg, Germany

[2] Minerva Center and Department of Physics, Bar-Ilan University, Ramat Gan, 52900 Israel

E-mail: stephan.reitzenstein@physik.tu-berlin.de

New Journal of Physics **15** (2013) 025030 (17pp)
Received 1 November 2012
Published 22 February 2013
Online at http://www.njp.org/
doi:10.1088/1367-2630/15/2/025030

Abstract. We report on electrically pumped quantum dot–microlasers in the presence of polarized self-feedback. The high-β microlasers show two orthogonal, linearly polarized emission modes which are coupled via the common gain medium. This coupling is explained in terms of gain competition between the two lasing modes and leads to distinct differences in their input–output characteristics. By applying polarized self-feedback via an external mirror, we are able to control the laser characteristics of the emission modes in terms of the output power, the coherence time and the photon statistics. We find that linearly polarized self-feedback stabilizes the lasing of a given mode, while cross-polarized feedback between the two modes reduces strongly the intensity of the other emission mode showing particular high-intensity fluctuations and even super-thermal values of the photon autocorrelation function $g^{(2)}(\tau)$ at

[3] Present address: Institut für Festkörperphysik, Technische Universität Berlin, Hardenbergstraße 36, D-10623 Berlin, Germany.

[4] Author to whom any correspondence should be addressed

Content from this work may be used under the terms of the Creative Commons Attribution 3.0 licence. Any further distribution of this work must maintain attribution to the author(s) and the title of the work, journal citation and DOI.

© IOP Publishing Ltd and Deutsche Physikalische Gesellschaft

zero delay. Measurements of $g^{(2)}(\tau)$ under external feedback also allow us to detect revival peaks associated with the round trip time of the external cavity. Analyzing the damping and shape of the $g^{(2)}(\tau)$ revival peaks by a phenomenological model provides us insight into the underlying physics such as the effective exciton lifetime and gain characteristics of the quantum dots in the active region of these microlasers.

Contents

1. Introduction

The search for an ultimate semiconductor nanolaser has triggered enormous research activities in the field of modern quantum optics [1]. Particular attention has been directed toward micro- and nano-lasers with low numbers of quantum dots (QDs) in the active region. Due to their small mode volume and high quality (Q) factors of the resonator, these lasers exploit cavity quantum electrodynamics (cQED) effects to achieve high spontaneous emission coupling (β) factors. Indeed, compared to conventional laser diodes with $\beta \approx 10^{-5}$, microlasers show β-factors close to unity, which allows one to reduce the laser threshold by orders of magnitude [2, 3], and threshold-less lasing is within the reach of current technology [4]. Moreover, the high fraction of spontaneous emission coupled into the lasing mode even facilitates the observation of single QD lasing effects in the weak coupling regime [5–7] and in the strong coupling regime [8] of cQED. Measuring the second-order photon autocorrelation function $g^{(2)}(\tau)$ of emission from such lasers has become an important method for identifying their operation mode and for distinguishing between a non-classical single QD regime ($g^{(2)}(0) < 0.5$), and the thermal ($g^{(2)}(0) = 2$) as well as coherent $g^{(2)}(0) = 1$ emission of light [6, 7, 9, 10].

Recently, the work on QD–microcavities was extended to systems controlled by external feedback which reveal striking features such as super-thermal bunching associated with $g^{(2)}(0) > 3$ [11], and theoretical studies even show that the strong coupling regime can be stabilized by delayed single photon feedback [12]. Furthermore, externally coupled sources of coherent light are of special relevance for fundamental questions of nonlinear dynamics, which has been studied extensively for conventional semiconductor laser diodes (see, e.g., reviews in [13, 14]). Self-feedback and synchronization of feedback-coupled optical systems also has an impact on applications and can, e.g., be exploited for the realization of ultra-fast random bit

generators [15], for secure data communication with chaotic pulses [16] or even for advanced information processing [17].

In this work, we report a detailed study of feedback-coupled QD–micropillar lasers. These electrically driven microlasers, which are based on the gain provided by a low number of QDs (of the order of a few tens QDs), feature high β-factors exceeding 0.1, threshold currents in the μA range and sub-μW output powers [18]. As such, they allow us to address an operation regime characterized by a limited QD gain medium and enhanced contribution of spontaneous emission, which is not accessible with conventional laser diodes based on quantum wells in the active medium and with mW output powers. Of particular interest for the present work is the presence of two orthogonal, linearly polarized radiation modes of the micropillar laser and the dependence of their emission features on polarized self-feedback. In fact, we find that polarized self-feedback can stabilize or disturb laser action of the emission modes which compete for the limited gain provided by the QDs in the active layer. It turns out that measuring the $g^{(2)}(\tau)$-function is a sensitive tool for investigating the effect of polarized feedback and, moreover, it gives important insight into the underlying dynamics by analyzing $g^{(2)}(\tau)$-revival peaks delayed by the round-trip time of the external cavity. In light of this, our work addresses a rather unexplored field of nanophotonics with high potential for various applications in the field of nonlinear optics and for inspiring research on nonlinear dynamics beyond the standard Lang–Kobayashi rate-equations model [19].

2. Sample preparation and experimental setup

External feedback coupling is studied on high-quality electrically pumped QD–microlasers, which are based on a planar microcavity structure grown by molecular beam epitaxy. The planar structure is composed of an n-doped GaAs substrate followed by an n-doped lower distributed Bragg reflector (DBR) with 27 alternating $\lambda/4$-thick AlAs/GaAs mirror pairs, an intrinsic one-λ-thick GaAs cavity layer and a p-doped upper DBR with 23 $\lambda/4$-thick AlAs/GaAs mirror pairs. The gain region consisting of a single, low-density layer of $In_{0.3}Ga_{0.7}As$ QDs with a density of $5 \times 10^9\,cm^{-2}$ is placed in the center of the GaAs cavity layer. This gives a total number of about 500 QDs in the active layer of micropillar lasers with a diameter of about 3.6 μm, as used in this study. However, a significantly lower number of QDs contributes effectively to lasing due to spectral and spatial mismatch. While the exact number of contributing QDs is difficult to determine experimentally, theoretical studies for a similar microlaser from the same wafer material indicate that the lasing is sustained by about 40 QDs [20]. Several nanotechnology processing steps including electron-beam lithography, plasma etching, planarization and the formation of the upper ring contact are performed in order to realize high-quality electrically contacted micropillar lasers. For details of the fabrication process see [21, 22]. The microlasers are investigated at low temperature ($\approx$20 K) using the micro-electroluminescence (μEL) setup (spectral resolution 30 μeV at 1.4 eV) equipped with a fiber-coupled Hanbury-Brown and Twiss (HBT) setup (temporal resolution 40 ps). External feedback is realized by a 90/10 beam splitter placed on the optical axis of the μEL setup (cf figure 1(b)). This beam splitter allows us to direct 90% of the collected light to an external mirror (10% of the light is transmitted to the spectrometer) that is placed at a variable distance l_{ext} away from the microlaser and defines the external cavity. The linear polarizers LP1 and LP2 allow for polarization-selective detection of light and for polarization-controlled feedback, respectively. The absolute output power of the microlaser can be determined by a power-meter placed in the detection path.

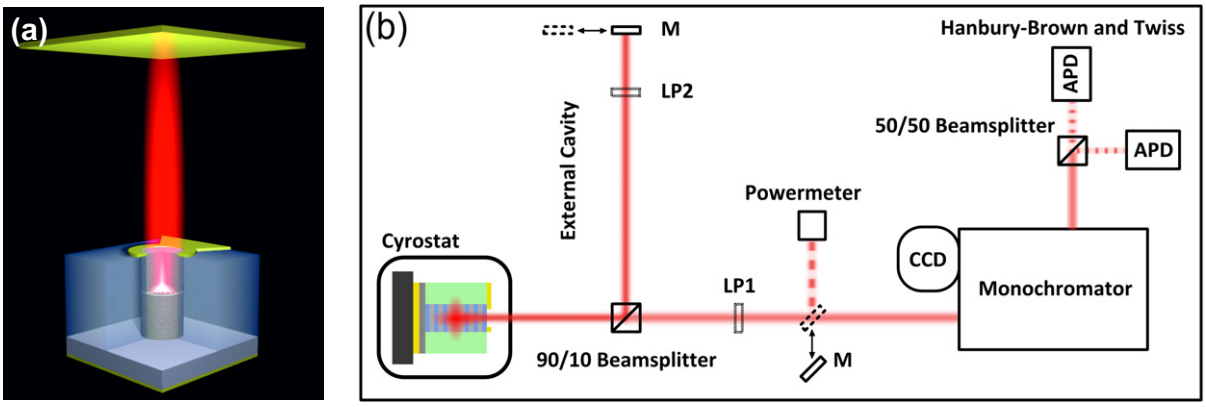

Figure 1. (a) Schematic image of an electrically pumped QD–micropillar in the presence of external feedback coupling. (b) Sketch of the μEL setup used for studying externally coupled microlasers (abbreviations: linear polarizer (LP), mirror (M), charge coupled device (CCD) and avalanche photo diode (APD)).

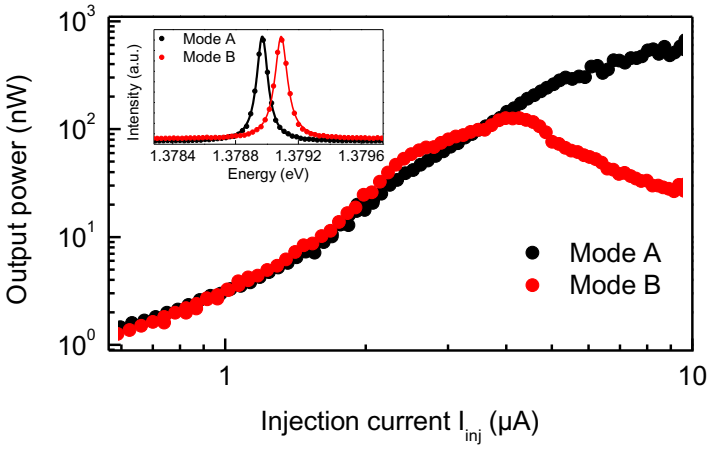

Figure 2. Output characteristic of the two orthogonal, linearly polarized emission modes A and B of a microlaser with a diameter of 3.6 μm as a function of injection current I_{inj}. Inset: polarization-resolved μEL emission spectra of the laser modes at $I_{\mathrm{inj}} = 0.9\,\mu$A, i.e. close to the threshold injection current.

3. Input–output characteristics of micropillar lasers without external feedback

Let us first address the input–output characteristics of the microlaser under study without external feedback coupling. The microlaser has a diameter of 3.6 μm and shows laser emission from the fundamental cavity mode at about 1.3790 eV. As can be seen from the μEL spectra displayed in figure 2 (inset), the twofold degeneracy which would be expected for this mode in the case of a resonator with a perfect circular cross-section is lifted and two orthogonal, linearly polarized components (modes A and B) are observed [23]. We would like to note that the observed splitting could in part also be attributed to an (unintended) asymmetry of the upper ring contact. The two emission modes are characterized by Q-factors of 19 900 (mode A) and 16 700 (mode B) at lasing threshold and have a spectral splitting of 133 μeV.

The two emission modes show distinct differences in the laser characteristics as presented in figure 2 on the log–log scale. The sub-microwatt output power of mode A shows a typical s-shaped dependence on the injection current I_{inj} with a smooth transition from spontaneous emission to stimulated emission at a threshold current of $I_{th,A} = 1.1\,\mu$eV. In contrast, the output power of mode B saturates above its threshold current of $I_{th,B} = 0.9\,\mu$eV at an emission power of about 100 nW and even decreases for injection currents exceeding $4\,\mu$A. This particular behavior has been observed before for conventional vertical cavity surface emitting lasers (VCSEL) and for micropillar lasers and is interpreted in terms of gain competition between the two modes [11, 24]. This interpretation is in agreement with slightly different Q-factors for the emission modes (see above) which reflect larger optical losses for mode B. It is also confirmed by theoretical studies based on a microscopic semiconductor laser theory [20]. Interestingly, mode B shows higher intensity than mode A in an intermediate injection regime from 2.0 to $3.5\,\mu$A. This can possibly be attributed to a slight overlap between the modes and the asymmetric Au ring contact and related absorption losses which are different for mode A and mode B and vary with excitation power.

4. Input–output characteristics of micropillar lasers with polarized external feedback

The effect of external feedback coupling on the input–output characteristics of microlasers is investigated by installing a polarization maintaining 90/10 beam-splitter (cf figure 1) into the optical axis. Figure 3(a) compares the input–output characteristics of the microlaser under investigation with and without external feedback in double logarithmic scale. To begin with, no polarizer is installed in front of the external mirror in order to provide full feedback. For both modes, the overall input–output characteristic is qualitatively independent of the feedback: mode A exhibits an s-shaped dependence of the output power as a function of the injection current, while mode B shows saturation and a decrease of the output power at high injection currents. A closer look reveals that above the laser threshold, external feedback leads to a reduction of the output power in the case of mode A by up to 35% at $I_{inj} = 7.8\,\mu$A. This change in output power reflects that the feedback disturbs the laser action which can, e.g., lead to chaotic behavior of the coupled microlaser–external mirror system [11]. The same holds true for mode B which also shows lower output intensity (by up to 33% at $I_{inj} = 7.9\,\mu$A) in the presence of external feedback.

The dependence of the laser characteristic on the feedback becomes more complex when a linear polarizer (LP2, cf figure 1) is installed in front of the external mirror, so that linearly polarized light can be selectively coupled back to one or the other mode. This gives us four possible feedback and detection configurations: (i) detection of mode A under feedback from mode A, (ii) detection of mode A under feedback from mode B, (iii) detection of mode B under feedback from mode B and (iv) detection of mode B under feedback from mode A. The respective input–output traces are depicted in figure 3(b).

Co-polarized coupling of the emission from mode A to the same mode in configuration (i) results in an s-shaped laser characteristic similar to that presented in figure 2(a) for full feedback. This behavior can be expected as long as the output power of mode A is significantly stronger than that of mode B under full feedback, so that photons coupled back from mode B play a minor role. In contrast, strong deviation from the s-shaped laser characteristic is observed when cross-polarized light from mode B is coupled back to the laser in configuration (ii), in which photons from mode A are blocked by the linear polarizer LP2. Naively, one might expect that feedback

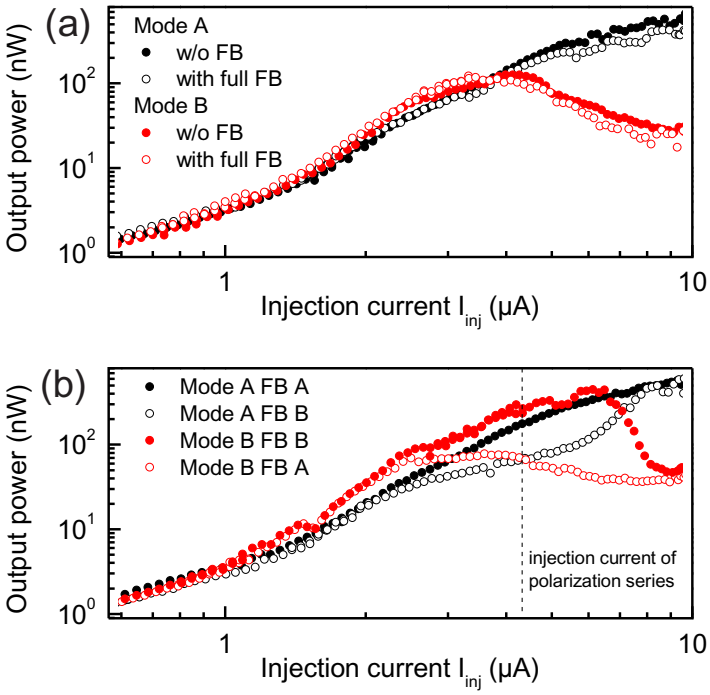

Figure 3. Output characteristics of modes A and B of the micropillar laser with different external feedback (FB) configurations: (a) modes A and B each with full (unpolarized) feedback and without feedback; (b) modes A and B each with co-polarized feedback and cross-polarized feedback, respectively. The vertical line in panel (b) indicates the injection currents at which the polarization-resolved photon correlation measurements presented in figure 8 were carried out.

from mode B with a significantly lower intensity should not influence the laser characteristic of mode A. However, as can be seen in figure 3(b), selective cross-polarized feedback coupling from mode B strongly reduces the output power of mode A in the current range from 2.5 to 7.0 μA. This effect is most pronounced at $I_{\mathrm{inj}} = 5.5\,\mu$A, where the intensity of mode A drops by a factor of 3.1 when photons from mode B effectively disturb the laser action of mode A.

Further insight into the effect of polarized feedback is obtained in configurations (iii) and (iv) where the laser characteristic of mode B is studied. The respective input–output traces are plotted in figure 3(b). Interestingly, co-polarized feedback realized in configuration (iii) clearly stabilizes laser action in mode B and leads to enhanced emission in the current range from 2.5 to 7.0 μA, as compared to the cases of full feedback or without feedback. Eventually, for injection currents exceeding 7.0 μA, the output power of mode B decreases strongly also in configuration (iii) and approaches values observed with full feedback coupling. The latter is attributed to larger optical losses of mode B, which cannot be compensated for by co-polarized feedback for injection currents exceeding a critical value. Again, cross-polarized self-feedback from mode B in configuration (iv) results in similar behavior to full feedback, i.e. saturation and a decrease of the output power for $I_{\mathrm{inj}} > 2.5\,\mu$A.

The overall lasing characteristics under polarization selective feedback can be understood in terms of the competition of two orthogonal modes for a common, limited QD gain medium [20]. First of all, one has to consider that coupling back only photons of one specific

mode increases the photon population of the respective mode inside the microresonator, which results in enhanced stimulated emission into this mode. This, in turn, reduces the available gain for the orthogonal mode and leads to a decrease of its output power. This effect is most pronounced in configuration (iii) when mode B is stabilized by co-polarized self-feedback while the output power of mode A is reduced due to lower effective gain.

5. Second-order photon autocorrelation from microlasers with polarized external feedback

In this section we discuss the photon statistics of a microlaser and compare the cases with and without external feedback. Moreover, we also address the effect of polarized feedback on the photon statistics. The photon statistics of emission is determined experimentally via a fiber-coupled HBT setup by measuring the second-order photon autocorrelation function $g^{(2)}(\tau)$, which gives important information about the emission process and allows one to distinguish, e.g., between a predominantly thermal light source with $1 < g^{(2)}(0) \leqslant 2$ and light generated by stimulated emission with $g^{(2)}(0) = 1$ [25]. In addition, by measuring the second-order photon auto-correlation function $g^{(2)}(\tau)$ one can also study the coherence properties of light: under the assumptions that the output intensity of the beam is time independent and that the lineshape is Lorentzian, the correlation function is given via $g^{(2)}(\tau)$ [26]

$$g^{(2)}(\tau) = 1 + (g^{(2)}(0) - 1)\, \mathrm{e}^{-2|\tau|/\tau_c}, \tag{1}$$

where τ_c is the coherence time of the light. For uncoupled microlasers it is well known that the smooth transition from thermal to coherent light with increasing pump current is associated with bunching behavior with $g^{(2)}(0) > 1$ near threshold [9, 10]. Well below threshold, in the regime dominated by spontaneous emission, the expected photon bunching with $g^{(2)}(0)$ approaching 2 can typically not be resolved due to the limited temporal resolution of standard APD-based HBT setups—an issue which can be circumvented by using a streak-camera as the detector [27].

First, we study and compare the photon statistics of a micropillar laser under full feedback and compare it with the case without feedback coupling. Figure 4(a) shows the photon autocorrelation function of mode A with and without external feedback at an injection current of 3.3 μA, i.e. slightly above threshold. In both cases, we observe clear photon bunching as an indication of the emission of thermal light. A closer look reveals distinct differences between the two traces: (a) in the presence of external feedback coupling the bunching value is narrower and (b) damped revival peaks appear at integer values of the round trip time $\tau_{ext} = 5.99$ ns in the external cavity. While (a) indicates a lower coherence time in the presence of external feedback, (b) reflects the emission of thermal light whose photons also correlate at integer multiples of τ_{ext}. In each round trip, part of the photons are coupled out of the external cavity by the 90/10 beam splitter or are lost otherwise, which explains the damping of the revival peaks. The photon autocorrelation function was measured also for a wider range of injection currents from close to the threshold up to the full lasing regime. The corresponding values of $g^{(2)}(0)$ and τ_c are summarized in figure 4(c). The transition from spontaneous emission to coherent laser emission is associated with a decrease of $g^{(2)}(0)$, which is hardly influenced by external feedback. In contrast, the coherence time determined from the $g^{(2)}(\tau)$ data according to equation (1) is more sensitive to external perturbations, which is reflected in significantly lower τ_c-values in the presence of external feedback, as can be seen in figure 4(c). A similar effect has also been observed in the laser regime for VCSELs with external feedback and is termed coherence collapse [28, 29].

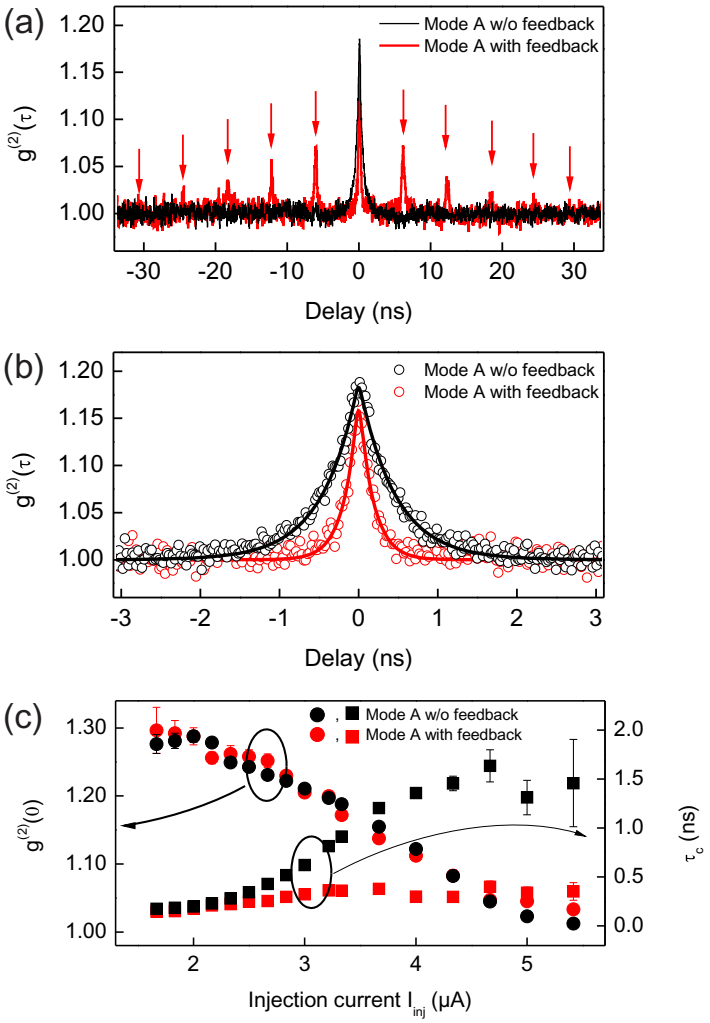

Figure 4. (a) Photon autocorrelation function $g^{(2)}(\tau)$ of mode A with and without external feedback at $I_{\mathrm{inj}} = 3.33\,\mu$A and $l_{\mathrm{ext}} = (1.79 \pm 0.01)$ m. Feedback leads to damped revival peaks (indicated by arrows) which are separated by the round-trip time $\tau_{\mathrm{ext}} = l_{\mathrm{ext}}/c = 5.99$ ns. (b) Zoom-in view of the correlation peak at zero delay. (c) Values of the second-order correlation function at zero time delay $g^{(2)}(\tau = 0)$ and coherence time τ_{c} with and without feedback versus injection current I_{inj}.

Next we study the photon statistics for injection currents well above the threshold current at $I_{\mathrm{inj}} = 33.3\,\mu$A. Here, the emission of coherent light should be reflected in $g^{(2)}(\tau) = 1$, which is exactly what we observe for mode A in the absence of feedback in figures 5(a) and (b). On the other hand, when photons are coupled back into the microlaser via the external cavity, the correlation function changes significantly and a pronounced bunching peak at $\tau \to 0$ as well as damped revival peaks form at integer values of the round-trip time. These bunching features need to be distinguished from the thermal bunching discussed before and can be attributed to the presence of a chaotic waveform in the external cavity [11]. Figure 5(c) summarizes the correlation values and the coherence time τ_{c} (with feedback) for a broader range of injection

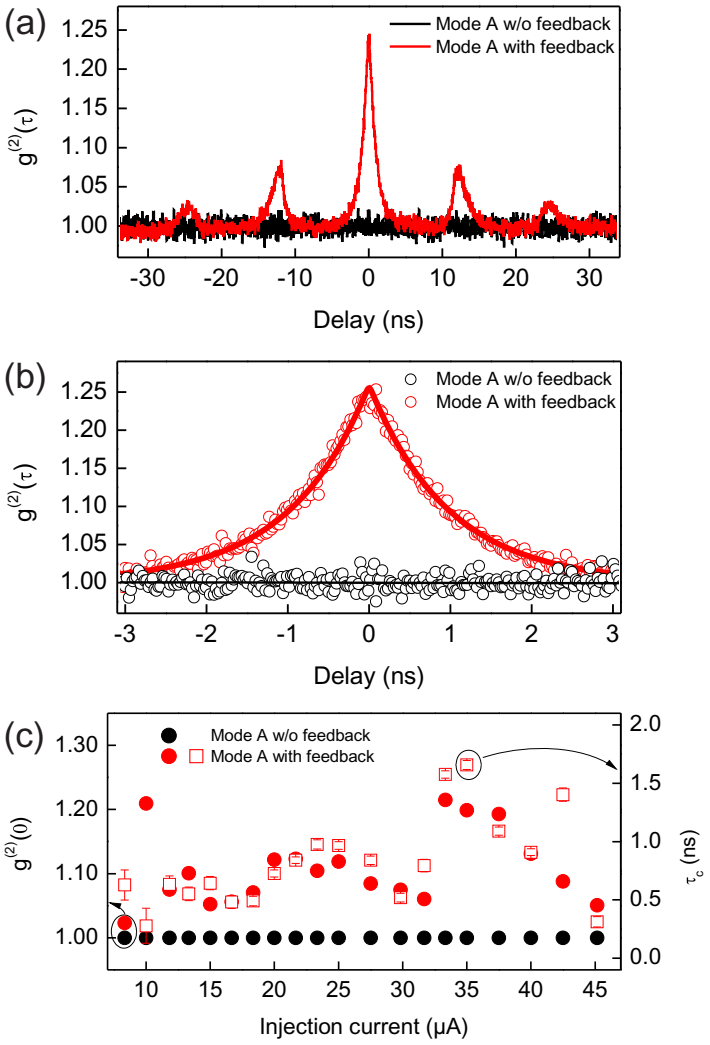

Figure 5. (a) Photon autocorrelation function $g^{(2)}(\tau)$ of mode A with and without external feedback at $I_{\mathrm{inj}} = 33.3\,\mu$A and $l_{\mathrm{ext}} = 3.49$ m ($\tau_{\mathrm{ext}} = 11.6$ ns). The damped revival peaks feature an asymmetric shape with a steeper flank toward small absolute delay times. (b) Zoom-in view of the correlation peak at zero delay. (c) Values of the second-order correlation function at zero time delay $g^{(2)}(\tau = 0)$ with and without feedback and coherence time τ_{c} with feedback versus injection current I_{inj}.

currents well above the threshold. In the whole range, feedback leads to enhanced temporal intensity fluctuations associated with $g^{(2)}(0) > 1$. We would like to note that the large spread of $g^{(2)}(0)$ and τ_{c} is not related to statistical variations, but reflects the high sensitivity of this quantity to the particular feedback configuration, which can, e.g., be influenced by slight temperature variations in the laboratory. This sensitivity becomes increasingly important at large injection currents. The occurrence of revival peaks in $g^{(2)}(\tau)$ is further illustrated in figure 6 where the photon autocorrelation function is compared for two external cavity lengths $l_{\mathrm{ext}} = 3.49 \pm 0.02$ and 1.79 ± 0.01 m. In both cases, a train of bunching peaks separated by $\tau_{\mathrm{ext}} = (11.63 \pm 0.06)$ and (5.99 ± 0.01) ns, respectively, is observed in agreement with

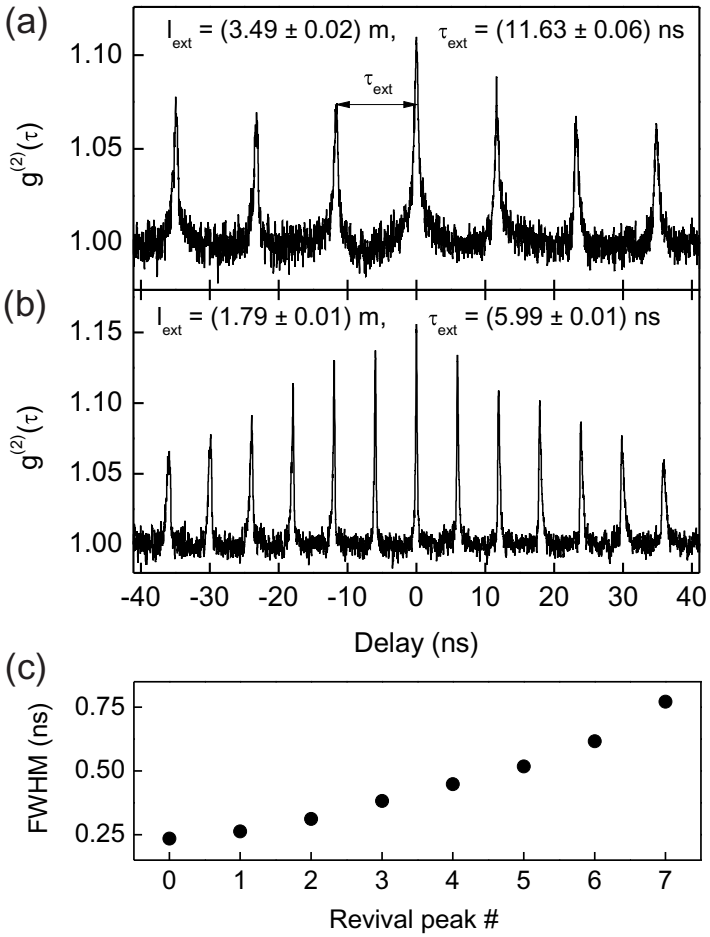

Figure 6. Comparison of the $g^{(2)}(\tau)$-functions for different external cavity lengths of $l_{\text{ext}} = (3.94 \pm 0.02)$ m (a) and $l_{\text{ext}} = (1.79 \pm 0.01)$ m (b), respectively. The corresponding round-trip times τ_{ext} are given in the figure. (c) Width (full-width at half-maximum) of the revival peaks versus the order n of revival.

$\tau_{\text{ext}} = l_{\text{ext}}/c$. It is interesting to note that the revival peaks have an asymmetric lineshape with a steeper flank toward $\tau = 0$ (see also figure 5(a)). This feature and the observed broadening of the peaks with the order of revival (cf figure 6(c)) allow one to explore some characteristics of the underlying dynamics and will be discussed in more detail in section 6.

Further insight into the nonlinear properties of the feedback-coupled microlaser is obtained by studying the $g^{(2)}(\tau)$-function of mode B for various injection currents above the laser threshold. The corresponding results are presented in figures 7(a)–(d), where $g^{(2)}(\tau)$ is plotted for two different injection currents with and without full feedback. The associated $g^{(2)}(0)$-values and the coherence times τ_c are depicted in figures 7(e) and (f). Similar to figure 5, photon bunching and the existence of revival peaks separated by $\tau_{\text{ext}} = 11.6$ ns can be observed in the presence of external feedback. However, there are also distinct differences between modes A and B. First of all, the bunching values are significantly larger for mode B, where super-thermal values exceeding $g^{(2)}(0) = 2$ appear in a wide range of injection and a maximum value of $g^{(2)}(0) = 3.5$ is detected at $I_{\text{inj}} = 6.7\,\mu$A as can be seen in figure 7(b). Interestingly, and in

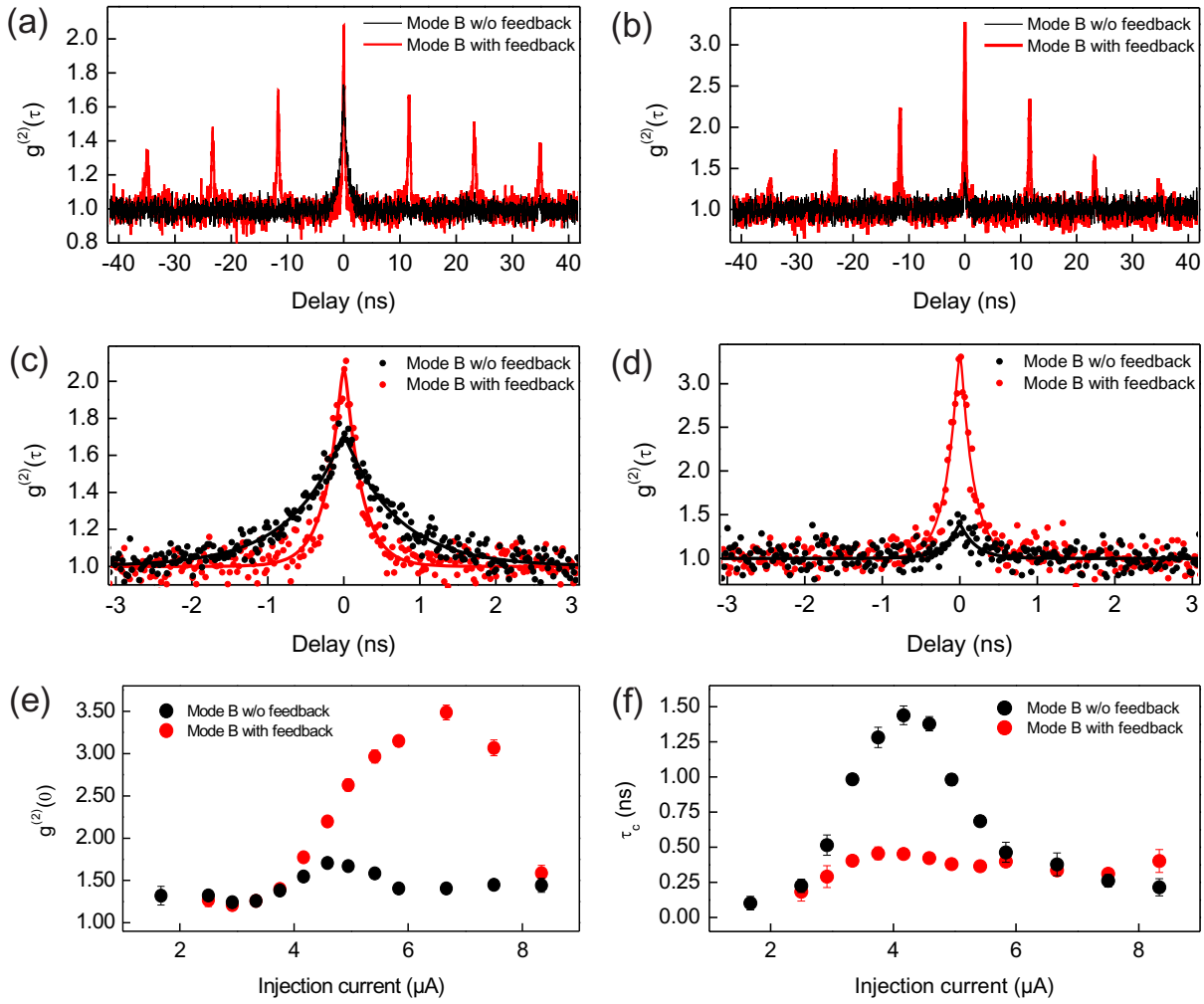

Figure 7. $g^{(2)}(\tau)$-functions of mode B with and without full feedback at $I_{\mathrm{inj}} = 4.6\,\mu$A ((a) and (c)) and $I_{\mathrm{inj}} = 6.7\,\mu$A ((b) and (d)), respectively ($l_{\mathrm{ext}} = 3.49$ m, $\tau_{\mathrm{ext}} = 11.6$ ns). The corresponding $g^{(2)}(0)$-values (e) and coherence time τ_{c} (f) as a function of injection current.

contrast to mode A, photon bunching occurs also without feedback, which indicates a significant fraction of spontaneously emitted photons in mode B. This is in agreement with the decreasing output intensity of mode B in the respective current range (cf figures 2 and 3(a)), indicating a reduction of stimulated emission in mode B with increasing injection current. The width of the bunching peaks with and without feedback is strongly different, which is nicely seen for the $g^{(2)}(\tau)$-function presented in figure 7(c) and in the extracted data plotted in figure 7(f) for a wider range of injection currents. The coherence time for the measurement without feedback reaches up to 1.4 ns at an injection current of 4.2 μA. This coincides with 1.4 ns extracted for the lasing mode A at the same current, which indicates that coherence is built up in both modes to a similar extent until mode A succeeds in the gain competition for $I_{\mathrm{inj}} > 4\,\mu$A above which stimulated emission in mode B is quenched. While the coherence time of mode B shows a pronounced dependence on I_{inj} in the absence of feedback, τ_{c} with feedback is almost constant with $\tau_{\mathrm{c}} \approx 0.4$ ns for $I_{\mathrm{inj}} > 4\,\mu$A, i.e. in the current range where a large super-thermal bunching

is observed (cf figure 7(e)). It is important to note that in this regime τ_c cannot be identified with the coherence time of emission—as in the case of thermal bunching—but rather represents the average timescale of individual chaotic pulses.

Instead of coupling photons of a specific mode back into the laser cavity in configurations (i)–(iv), it is also possible to adjust the angle ϕ of the linear polarization filter in the external cavity gradually. The polarization-dependent measurements shown were performed with an injection current of $I = 4.2\,\mu$A.

The corresponding polarization angle ϕ-dependent correlation values of mode A $g_A^{(2)}(0,\,\phi)$ are depicted in figure 8(a). The figure also includes $g_A^{(2)}(0)$-values of the laser emission with full feedback and without feedback as a reference (black and blue circles, respectively). They are approximately equal, indicating that the $g_A^{(2)}(0) > 1$ values stem mainly from thermal emission (cf figure 4(c)). Polarized feedback in the direction of modes A and B, respectively, equates to 90° and 0° as indicated by arrows in the upper right corner of the figure. Angles $\phi = 45°$, 135°, 225° and 315° imply that the polarization filter suppresses equal amounts of modes A and B and, therefore, effectively weakens the unpolarized feedback. This is in agreement with the observation that at those angles the $g_A^{(2)}(0,\,\phi)$ curve intersects the reference circle of unpolarized, i.e. full, feedback. When the filter is turned in the direction of the orthogonal mode B, the $g_A^{(2)}(0,\,\phi)$ values increase distinctly. This behavior can be explained by an enhanced fraction of thermal light in the emission of mode A, which is again consistent with the decrease of output intensity in this configuration as can be seen in figure 3(b). However, results presented below for mode B imply that also chaotic intensity fluctuations introduced through polarized feedback play an important role. On the other hand, when the filter is turned toward the polarization of mode A, feedback stabilizes laser action of mode A and $g_A^{(2)}(0,\,\phi)$ approaches the coherent limit $g^{(2)}(0) \to 1$.

Mode B shows a qualitatively similar $g_B^{(2)}(0,\,\phi)$ curve, as displayed in figure 8(b). However, the sensitivity of $g_B^{(2)}(0)$ to the feedback configuration is significantly more pronounced. First of all, comparing the $g_B^{(2)}(0)$ values with and without full feedback of photons into the microlaser cavity reveals significantly larger $g_B^{(2)}(0)$ if full feedback is applied, indicating the onset of the regime of chaotic pulsing behavior (see the discussion regarding figure 8(e)). The $g_B^{(2)}(0,\,\phi)$ curve of mode B is analogous to the 90° tilted curve of mode A. As discussed above, co-polarized feedback stabilizes laser action and leads to $g_B^{(2)}(0)$-values approaching unity at 0° and 180°. In contrast, cross-polarized feedback enhances the intensity fluctuations and results in maximum $g_B^{(2)}(0,\,\phi)$-values at angles of approximately 90° and 270°, which are slightly larger than 2 (cf the green circle in figure 8(b)) and therefore can not be attributed to thermal light alone.

Similar to the results discussed in [11] with $g^{(2)}(0)$-values exceeding 2, the polarization-dependent $g^{(2)}(0,\,\phi)$ curves of mode B show super-thermal bunching for polarized feedback from mode A. Obviously, this behavior is most pronounced for the microlaser with external feedback when the regarded mode is dominated by the other, orthogonal mode. In order to explain the behavior of the suppressed mode to exhibit a time-dependent emission characteristic, an interaction between the two modes needs to be present. Most probably this coupling of photons from modes with orthogonal polarization is mediated by the QD gain medium as mentioned above, and the enhanced intensity fluctuations of the suppressed modes reflected in large $g^{(2)}(0)$-values can be explained as follows: via competition of the two modes for the limited few-QD gain medium, one of the modes (depending on which mode is coupled back into the resonator) dominates over the other and thereby defines the stimulated emission of the

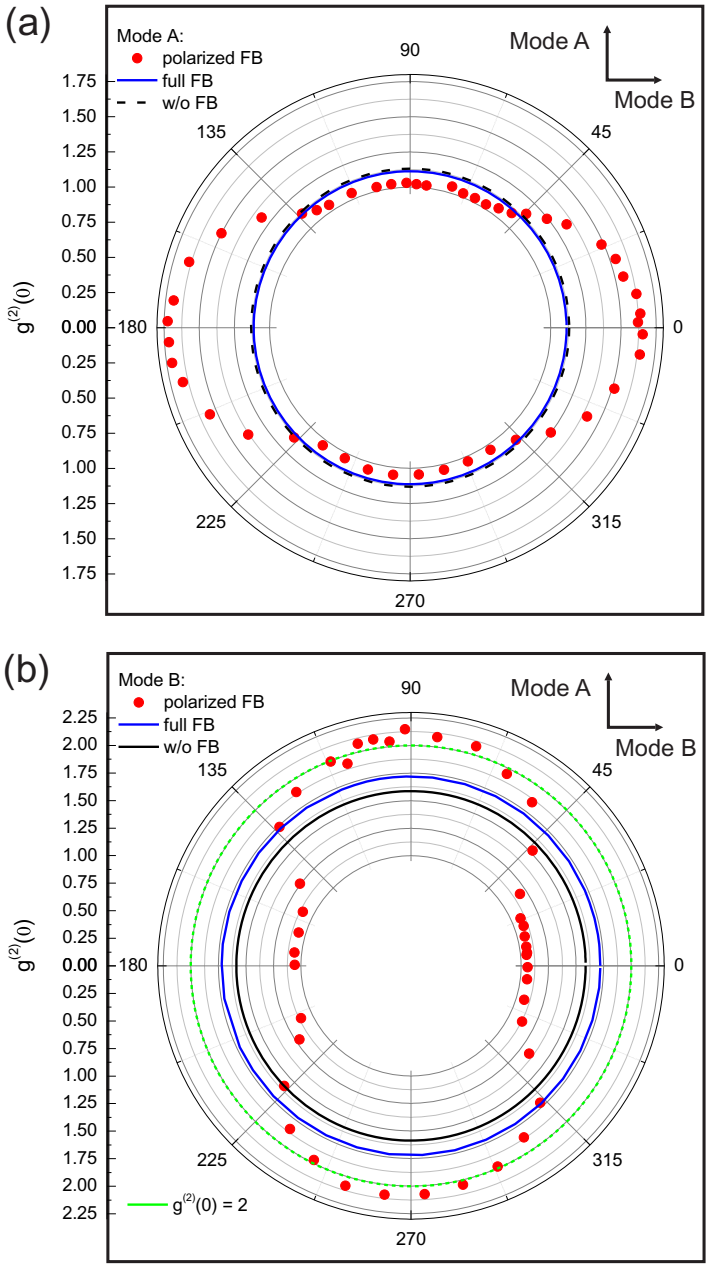

Figure 8. Values of the second-order correlation function at zero time delay $g^{(2)}(\tau = 0, \phi)$ as a function of the angle ϕ of the polarization filter in the external cavity for (a) mode A and (b) mode B at $I_{\text{inj}} = 4.2\,\mu$A. The orientation of polarized feedback with respect to the polarization of mode A (90° and 270°) and mode B (0° and 180°) is indicated by arrows in the upper right corners. Reference data for full feedback (blue circle) and without feedback (black circle) are also shown.

microlaser. Random statistical fluctuations of the suppressed mode are enhanced as a fraction of the fluctuations are reflected back into the laser cavity. Those reentering fluctuations, in turn, tip the balance of the photon populations in favor of the suppressed mode for a short

time interval. As the average balance of the photon population remains the same, the emission of the suppressed mode is condensed into seemingly random spikes (that are quasi-periodic with the external cavity round-trip time τ_{ext}). Similar chaotic behavior has been observed in semiconductor laser diodes with external cavities [30, 31]. The output characteristic of the dominant mode remains roughly stable.

6. Dynamical properties of feedback-coupled microlasers

As described above and displayed in figure 5(a), the photon autocorrelation function of feedback-coupled microlasers reveals distinct dynamical features in the shape of the revival peaks. In order to understand and analyze the underlying physical properties, we introduce a phenomenological model which considers the back-coupling of photons via an external mirror. In particular, the model takes into account four processes that can occur when a resonant photon is directed back to the microlaser: (a) the photon can be directly reflected by the microcavity; (b) the photon can enter the cavity and leave after the characteristic photon lifetime $\tau_{\text{cav}} = Q\hbar/E_{\text{c}}$ (Q is the cavity quality factor and E_{c} the resonant energy of the cavity), and while present in the cavity the photon can contribute to stimulated emission; (c) the photon can enter the cavity, be absorbed by a QD and be re-emitted via spontaneous or stimulated emission after a characteristic radiative lifetime τ_X; (d) the photon can be lost due to a number of processes such as diffraction, absorbtion by materials (other than QDs), etc.

Let us now analyze these processes and their impact on the shape of the revival peaks in more detail. It is clear that direct reflection of an incident photon pulse does not change its shape. On the other hand, photons entering the microcavity experience a delay before possible re-emission. The delay can simply be caused by the cavity lifetime τ_{cav} that is approximately 10 ps for the given structure. In addition, absorption and spontaneous or stimulated emission with a (combined) effective lifetime τ_X can take place. Both τ_{cav} and τ_X are statistical quantities and the associated photon delay times are distributed exponentially because the processes occur with a constant probability in a given time interval. Mathematically, the resulting shape of the revival peak is described by a convolution between the incoming pulse and the delay distribution. Moreover, if there are more photons in the re-emitted pulse than in the incoming one, the gain is larger than the loss and vice versa.

In a stationary case, the average optical gain should exactly compensate for all losses of a pulse for a full round trip in the external cavity. In the limit of vanishing gain correlation and by taking into account that light performing a round trip in the external cavity has to pass the 90/10 beam-splitter twice, only a maximum of 81% of the photons of one pulse at time t can be correlated with the subsequent pulse at time $t + \tau$. Thus, correlation values exceeding 81% would unambiguously indicate that a fraction of the photons from the incoming pulse enter the cavity and experience optical gain via stimulated emission.

In order to describe the shape of the nth revival peak of the photon autocorrelation function, we take into account that the cavity lifetime τ_{cav} is much smaller than the Purcell enhanced radiative exciton lifetime τ_X, which implies that the broadening of revival peaks due to τ_{cav} can be neglected. Moreover, since the shape of the central correlation peak at $\tau = 0$ is given by equation (1), the nth-order correlation peaks can therefore be approximated via

$$g^{(2)}_{n>0}(\tau_n) - 1 \simeq F_{\text{corr}} \left[A\,[g^{(2)}_{n-1}(\tau_n) - 1] + (1 - A)\,[g^{(2)}_{n-1}(\tau_n) - 1] * \Theta(\tau_n)\,\frac{\mathrm{e}^{-\frac{\tau_n}{\tau_X}}}{\tau_X} \right], \tag{2}$$

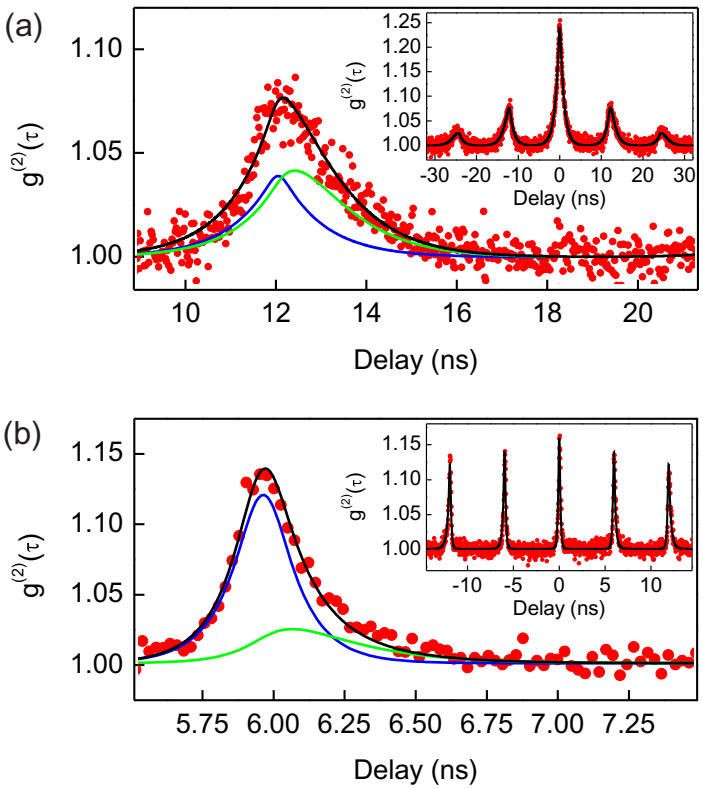

Figure 9. Modeling of photon autocorrelation function $g^{(2)}(\tau)$ according to equation (2). (a) Photon autocorrelation function obtained at $I_{\mathrm{inj}} = 33.3\,\mu$A and $l_{\mathrm{ext}} = 3.49$ m for mode A with full feedback. The temporal evolution of the revival peaks is well described by the model. Modeling the revival peaks up to second order, we obtain the best quantitative agreement for $F_{\mathrm{corr}} = 0.391 \pm 0.004$, $A = 0.42 \pm 0.09$ and $\tau_X = 0.64 \pm 0.06$ ns. (b) Experimental and theoretical $g^{(2)}(\tau)$ data for the same laser at $l_{\mathrm{ext}} = 1.79 \pm 0.01$ m and $I_{\mathrm{inj}} = 10.0\,\mu$A. Fitting the experimental data yields $F_{\mathrm{corr}} = 1.02 \pm 0.02$, $A = 0.74 \pm 0.02$ and $\tau_X = 0.22 \pm 0.02$ ns. In both panels the reflected part (blue line) as well as the absorbed and re-emitted part (green trace) are plotted separately to illustrate the composition of the revival peak.

where $\tau_n = \tau - n\,\tau_{\mathrm{ext}}$ is the retarded delay, Θ is the unit step function and A denotes the effectively reflected fraction of the incident pulse. Thus, $1 - A$ is the fraction of the pulse which is delayed due to absorbtion. The correlation parameter F_{corr} measures the total correlation between the photons of the $(n-1)$th and the nth bunching peak and is defined via

$$F^n_{\mathrm{corr}} = \frac{\int (g^{(2)}_n(\tau) - 1)\,\mathrm{d}\tau}{\int (g^{(2)}_{n-1}(\tau) - 1)\,\mathrm{d}\tau}. \tag{3}$$

As discussed previously, for the present feedback configuration with a 90/10 beam-splitter in the external cavity, the upper limit of F_{corr} is 0.81 in the absence of gain.

Equation (2) predicts an asymmetric broadening of the bunching peaks, which increases with the revival order $n > 0$, in good agreement with the data presented in figure 6(c). The applicability of this model to the experimental data is demonstrated in figure 9(a), which

shows the correlation function for mode A in the presence of external feedback at an injection current of 33.3 μA and an external cavity length of 3.49 m. In this case, the asymmetry of the revival peaks is very pronounced, which is illustrated exemplarily for the first revival peak ($n = 1$) at positive delay times. It can also be seen that the experimental data can nicely be described by our model (black curves in figure 9) according to equation (2) under variation of the parameters F_{corr}, A and τ_X. The best agreement with the experimental data was obtained for $F_{\mathrm{corr}} = 0.391 \pm 0.004$, $A = 0.42 \pm 0.09$ and $\tau_X = 0.64 \pm 0.06$ ns via modeling the revival peaks up to $n = \pm 2$. Using these parameters we are able to plot the reflected part (blue curve) of the incident pulse and the absorbed and re-emitted part (green curve) separately. As can be seen in figure 9(a) the asymmetry of the revival peak with a tail for a large delay time is caused by the absorbed and re-emitted part of the incident pulse. In this example the revival peaks are strongly damped, which is reflected in $F_{\mathrm{corr}} \ll 0.81$ and indicates a low gain contribution in the re-emitted part and/or large optical losses.

A significantly lower damping of the revival peaks is observed for the $g^{(2)}(\tau)$ curve displayed in figure 9(b) for the same microlaser at a lower injection current of 10.0 μA. The associated correlation parameter F_{corr} was determined by fitting the revival peaks up to an order of $n = \pm 2$. In agreement with the lower damping, a value $F_{\mathrm{corr}} = 1.02(2)$ ($A = 0.74 \pm 0.02$ and $\tau_X = 0.22 \pm 0.02$ ns) was obtained which is larger than the theoretical limit of $F_{\mathrm{corr}} \leqslant 0.81$ without gain. Therefore, the pulses cycling the external cavity are clearly enhanced by stimulated emission with each passing of the laser cavity. The lower gain contribution at the higher injection current is attributed to gain saturation effects which limit the amplification if the photons are entering the microlaser via external feedback.

The determined values of the effective, Purcell enhanced radiative exciton lifetime τ_X and hence the timescale of the re-emission process are of the order of a few hundreds of ps up to about 1 ns, which gives a bandwidth for chaotic switching events in the GHz range. As such, our measurements provide a unique opportunity to determine the effective Purcell effect, which considers the contributions of resonant *and* non-resonant QDs, under high excitation conditions in the lasing regime. In this context, the lower value of $\tau_X = 0.22$ ns at $I_{\mathrm{inj}} = 10\ \mu$A as compared to $\tau_X = 0.64$ ns at $I_{\mathrm{inj}} = 33\ \mu$A indicates that the Purcell enhancement is less pronounced at higher injection currents, which is attributed to power broadening of single exciton lines and the associated bleaching of the Purcell effect under high injection conditions [32]. We would like to note that even though our phenomenological approach (equation (2)) describes the observed asymmetric broadening of the revival peaks very well, it could possibly be improved by considering semiconductor-specific effects of the gain material in a more advanced model.

7. Conclusion

In summary, we have performed a detailed study of an electrically pumped QD–micropillar laser in the presence of polarized self-feedback. The two orthogonal linearly polarized emission modes of the laser show pronounced dependences on the external feedback coupling which are a function of the injection current, the length of the external cavity and the polarization of the feedback. Input–output characteristics revealed a coupling of the two modes mediated by the common gain material, and polarization selective feedback of emission allowed us to externally control the emission power of each mode by stabilizing or disturbing the laser action. We further showed that photon autocorrelation measurements are an important and sensitive tool to investigate the effect of polarized feedback on the optical properties of microlasers.

In particular, measurements of the photon autocorrelation function $g^{(2)}(\tau)$ reveal the existence of damped revival peaks separated by the round-trip time of the external cavity, which allowed us to address the interplay between reflection, absorption and re-submission and the underlying dynamics of light coupled back to the microlaser. As such, our studies give important insight into the rich and fascinating physics of feedback-coupled microlasers which could trigger further theoretical studies of this nonlinear dynamical system and could pave the way for novel, feedback-controlled microphotonic devices.

Acknowledgments

We thank M Emmerling and A Wolf for expert sample preparation. This work was financially supported by the DFG via research grant no. DFG Re2974/2-1 and the State of Bavaria.

References

[1] Noda S 2006 *Science* **314** 260
[2] Björk G and Yamamoto Y 1991 *IEEE J. Quantum Electron.* **27** 2386
[3] Björk G, Karlsson A and Yamamoto Y 1994 *Phys. Rev.* A **50** 1675
[4] Khajavikhan M *et al* 2012 *Nature* **482** 204
[5] Xie Z G *et al* 2007 *Phys. Rev. Lett.* **98** 117401
[6] Reitzenstein S *et al* 2008 *Opt. Express* **16** 4848
[7] Nomura M *et al* 2009 *Opt. Express* **17** 15975
[8] Nomura M *et al* 2010 *Nature Phys.* **6** 279
[9] Strauf S *et al* 2006 *Phys. Rev. Lett.* **96** 127404
[10] Ulrich S M *et al* 2007 *Phys. Rev. Lett.* **98** 043906
[11] Albert F *et al* 2011 *Nature Commun.* **2** 366
[12] Carmele A *et al* 2012 *Phys. Rev. Lett.* **110** 013601
[13] Petermann K 1995 *IEEE J. Sel. Top. Quantum Electron.* **1** 480
[14] van Tartwijk G H M and Agrawal G P 1998 *Prog. Quantum Electron.* **22** 43
[15] Kanter I *et al* 2005 *Nature Photon.* **4** 58
[16] Kinzel W and Kanter I 2007 *Handbook of Chaos Control* ed E Schoell and H G Schuster (New York: Wiley) pp 303–23
[17] Appeltant L *et al* 2011 *Nature Commun.* **2** 468
[18] Reitzenstein S *et al* 2008 *Appl. Phys. Lett.* **93** 061104
[19] Lang R and Kobayashi K 1980 *IEEE J. Quantum Electron.* **16** 347
[20] Leymann H A M 2013 arXiv:1301.3417
[21] Bockler C *et al* 2008 *Appl. Phys. Lett.* **92** 091107
[22] Reitzenstein S *et al* 2011 *IEEE J. Sel. Top. Quantum Electron.* **17** 1670
[23] Reitzenstein S *et al* 2007 *Appl. Phys. Lett.* **90** 251109
[24] Sondermann M *et al* 2003 *Phys. Rev.* A **68** 033822
[25] Glauber R J 1963 *Phys. Rev.* **130** 2529
[26] Loudon R 2000 *The Quantum Theory of Light* (Oxford: Oxford University Press)
[27] Wiersig J *et al* 2009 *Nature* **460** 245
[28] Lenstra D *et al* 1985 *IEEE J. Quantum Electron.* **21** 674
[29] Chung Y C and Lee Y H 1991 *IEEE Photon. Technol. Lett.* **3** 597
[30] Rosenbluh M *et al* 2007 *Phys. Rev.* E **76** 046207
[31] Uchida A *et al* 2008 *Nature Photon.* **2** 728
[32] Ulhaq A *et al* 2010 *Phys. Rev.* B **82** 045307